C.P. No. 1324

C.P. No. 1324

PROCUREMENT EXECUTIVE, MINISTRY OF DEFENCE

AERONAUTICAL RESEARCH COUNCIL

CURRENT PAPERS

An Assessment of the Accuracy of Subsonic Linearized Theory for the Design of Warped Slender Wings

bY

Patricia J. Davies

Aerodynamics *Dept.*, R.A.E., Farnborough

LONDON: HER MAJESTY'S STATIONERY OFFICE

1975

PRICE £1-80 **NET**

R. 48871

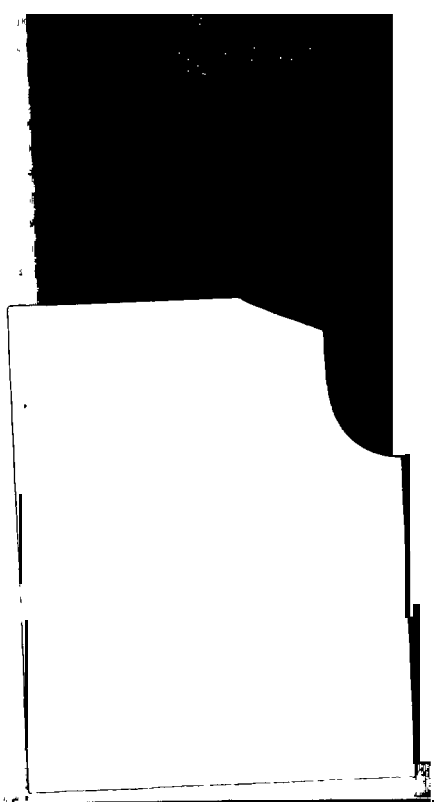

UDC 533.693.3 : 533.6.043.2 : 533.6.013.13 : 533.6.013.12 : 533.6.011.32

*CP No. 1324
October, 1973

AN ASSESSMENT OF THE ACCURACY OF SUBSONIC LINEARIZED THEORY FOR THE DESIGN OF WARPED SLENDER WINGS

by

Patricia J. Davies

SUMMARY

A series of warped slender wings has previously been designed using the linearized theory of subsonic flow, as a basis for a systematic experimental investigation of the drag reduction obtainable by warp at low speeds. The force measurements on these wings have now been supplemented by measurements of the pressure distribution over one of them; and the pressure distribution on it has also been calculated for inviscid incompressible flow by a surface-singularity method. This Report compares the distribution of pressure used in the design with those measured and calculated for the design incidence, at which the flow was attached; and assesses the validity of the linear theory. The chief weaknesses are found to be on the thicker cross-sections near the apex, and towards the trailing edge where boundary-layer effects become significant.

* Replaces RAE Technical Report 73159 - ARC 35314

CONTENTS

1 INTRODUCTION

Studies on the suitability of a slender all-wing type of aircraft for an airbus to carry two or three hundred passengers over short distances at subsonic speeds have included wind tunnel tests [1,2] on a series of typical wing shapes [3]. The principal aim of these tests was to investigate the increase in lift-to-drag ratio obtainable at lift coefficients typical of take-off conditions by warping (i.e. cambering and twisting) the wing.

In the design of the warped models, it was desired to keep the same orderly development of the flow as is obtained on a plane slender wing, in which the flow separates along the whole length of the leading edge above a very small angle of incidence, and forms coiled vortex sheets above the wing, maintaining this type of flow until some large incidence beyond the normal range of operating conditions. The addition of warp to the wing will generally disrupt this pattern and the flow will separate towards the upper and lower surfaces of the wing from different parts of the leading edge at low incidences, unless the type of warp is such that the wing has an attachment incidence. In this case, the flow will be attached over the whole wing at the attachment incidence, and will form coiled vortex sheets above the wing at any higher incidence.

As a general guideline, it has been found that lift is produced most efficiently at a lift coefficient about twice that at the attachment incidence. Thus, since at present we only have methods for designing wings at the attachment incidence, the wings were designed for attached flow at lift coefficients up to about half that required at the crucial operating condition, i.e. take-off, with properties at the design condition which would lead, it was hoped, to performance benefits at this operating condition. These properties included the avoidance of flow separation forward of the trailing edge, leading to an orderly development of the flow; a specified lift and centre of pressure; and a low vortex drag. Such a design can be carried out by the use of linear theory, which also has the important advantage as a design method of permitting the superposition of solutions and allowing the separation of lifting and thickness effects.

Linear theory was therefore used in the design of the series of models, which is described fully in Ref.3. The experimental force measurements on these wings are described in Ref.1 for the transition-free tests, and Ref.2 for the transition-fixed tests, from which the results in this paper have been taken.

In these experiments, flow-visualisation tests showed that the flow was attached at the design incidence and the lift coefficient obtained experimentally was very close to the design value, although the measured centre of pressure position was about 3% further forward than expected theoretically. In order to obtain a better assessment of the strengths and weaknesses of the linear theory, a pressure-plotting model of the first wing in the series was constructed and tested [4] in the No.2 11½ft wind-tunnel at RAE, Farnborough.

The pressure distribution on the same wing has also been calculated by Roberts and Rundle[5]. Their method constructs a solution of Laplace's equation, governing three-dimensional inviscid incompressible flow, by the use of singularity distributions on the surface of the wing and in a mean plane representing the wake. The wing surface is divided into four-sided elements, which satisfy smoothness conditions along their common sides,and a source distribution is defined on each, again satisfying smoothness conditions along the common sides. Planar doublet elements are used to represent the wake. The strengths of the source and doublet distributions are determined from conditions of zero normal velocity at the centres of the surface elements. The method represents an improvement over the fully-linearized theory used in the design process[3] in taking proper account of the finite thickness and warp of the wing. It also differs in being a direct calculation, producing the properties of a given shape, rather than a design calculation. Unfortunately, it does not fully represent the flow near a sharp leading edge: the strength of the source distribution on an element adjoinin,σ a sharp edge should vary in a way depending on the edge angle, but this has only been implemented for trailing-edge elements.

In this Report, the pressures, loads, lift and pitching moment given by the fully linearized treatment used for the design of the wing are compared with those given by the more nearly exact theory for inviscid flow and with those measured in the wind tunnel, at the design condition for which the flow is attached. Section 2 describes the wing, the procedure used to interpolate between the results of Roberts and Rundle to obtain values at the points on the wing at which the measurements were made, and the integration techniques used to obtain the overall lift and moment. An attempt to calculate the pressure drag from the results of Roberts and Rundle is also described. The results are presented and discussed in section 3 and some conclusions are drawn in section 4.

2 DETAILS OF CALCULATIONS

2.1 Description of the wing

The wing has a mild-gothic planform, which resembles a delta near the apex but has streamwise tips, and is shown in Fig.1. Using a Cartesian coordinate system (x,y,z), nondimensionalised with respect to the root chord c, with the x axis parallel to the undisturbed flow, the z axis passing through the apex and the y axis to starboard, the equation for the starboard leading edge is

$$Y = s(x) = \frac{s_T}{4}(5x-x5) \quad , \tag{1}$$

where s_T is the semispan at the trailing edge. The semispan of this wing is

$$s_T = 0.40385 \quad ,$$

giving an aspect ratio

$$A = 1.385 \quad ,$$

planform parameter

$$P = (\text{wing area})/(\text{span} \times \text{length}) = 7/12 \quad ,$$

and leading-edge sweep-back angle at the apex of $63^{\circ}13'$.

The wing has sharp, drooped leading edges, and a sharp, straight trailing edge given by $x = 1$, $z = 0$. The volume distribution has a thickness to chord ratio of 9% on the centre line and is illustrated in Fig.2, where the centre section and several cross-sections of the wing are drawn. The upper and lower surfaces are both continuously curved. The wing was designed by linear theory to have a lift coefficient of 0.1, and a centre of pressure at $x_{c.p.} = 0.533$, at the attachment incidence of 5.32'. This centre of pressure was chosen to coincide with an estimated position of the aerodynamic centre of the unwarped wing.

Full details of the design of the wing are given in Ref.3, where the wing is referred to as wing I. The three-component balance measurements are described in Refs.1 and 2, where the wing is referred to as wing B, and the pressure measurements are described in Ref.4.

2.2 Original format of the data

The static pressure holes in the wind tunnel model4 are located on cross-sections at every 10% of the centre line chord and at $x = 0.06$ and 0.95. On each cross-section there are holes at values of η at intervals of 0.1 from 0 to 0.9 and at $\eta = 0.95$, where $\eta = y/s(x)$ is the local non-dimensional spanwise coordinate. This grid of points is called the 'standard' grid, and is shown on the left of Fig.1. Pressure coefficients at the points of this grid have also been calculated by linearized theory.

The computer program of Roberts and Rundle[5] also employed a grid based on constant values of x and η, but the grid lines were concentrated near the apex, the trailing edge and the leading edges, as detailed in Appendix A. Interpolation was therefore required* in order to make effective comparisons with the experimental values on the standard grid. The values of the pressure coefficient calculated on the two grid lines nearest the leading edge were not sufficiently consistent for meaningful interpolation (see section 2.3) and so these two lines were ignored. The 17 lines of constant x and the remaining 11 lines of constant η on the half-wing are shown on the right of Fig.1. It is convenient to refer to this as 'Roberts grid'.

The computer output provided results at the design incidence of the wing and at an angle of incidence one degree larger.

2.3 The interpolation scheme

The pressure coefficients on each surface and at both incidences, given by the method of Ref.5, were interpolated to obtain values at the gridpoints of both Roberts' and the standard grid. This interpolation was carried out in two stages - first the interpolation to specified values of η at constant values of x and then the interpolation to specified values of x at constant values of η.

---

* In fact, the computer output quoted values of the velocity and pressure coefficient at slightly different sets of points on the upper and lower surfaces, the values of x being the same on the two surfaces, but the values of η being somewhat different, particularly where the wing is thick. Interpolation was therefore needed even to obtain values of the local load.

The calculated variation of the pressure coefficients with η becomes inconsistent very near the leading edges. This is illustrated in Fig.3 for the spanwise section $x = 0.8536$. The two points nearest the leading edge are not, however, points where the boundary condition has been satisfied in the course of the calculation, and it is not claimed that the pressure coefficients at these points are accurate. These two points have therefore not been used in the interpolation scheme. The pressure coefficients at the remaining 11 spanwise points generally display a smooth variation with η.

For the interpolation scheme, the local variation of the pressure coefficient with the coordinate x or η is assumed to be given by a cubic polynomial. Wherever possible, the pressure coefficient is taken as that given by the cubic polynomial fitted through the values of the pressure coefficient at the four neighbouring points, two on each side of the required point, at which it was provided in the computer output. However, where there are less than two points on one side of the required point, the cubic polynomial taken is that through the four nearest points. This slightly less accurate procedure is only necessary when the required point is near the leading edge. Extrapolation is required for some points on the lower surface, but here the variation of the pressure coefficients is generally smooth. The greatest variation of the pressure coefficients occurs near the leading edge on the upper surface, and here the cubic interpolation scheme produces better results than any of the other schemes tried.

Generally, the interpolation scheme produces results which appear to have an accuracy consistent with the accuracy of the original results. As an example the pressure coefficients interpolated at $\eta = 0.7$, 0.8, 0.9 and 0.95 on the cross-section $x = 0.8536$ are shown with flagged symbols in Fig.3.

The pressure distributions for the cross-sections at $x = 0.1$, 0.3, 0.5, 0.7 and 0.9 obtained by interpolating between the computed values in this way are shown in Fig.4 for the design incidence and for an incidence 1^{o} larger. They are discussed in section 3.4.

2.4 Calculation of load

The load $\ell(x,y)$ at a point (x,y) on the planform is given by

$$\ell(x,y) = Cp(x,y)\big|_{\text{lower surface}} - Cp(x,y)\big|_{\text{upper surface}} .$$

The load according to the nonlinear theory [5] has been calculated at each point on both Roberts and the standard grids, using the interpolated pressure coefficients. The distribution of load on the cross-sections x = 0.1, 0.3, 0.5, 0.7, 0.8 and 0.9 is illustrated by broken lines in Fig.5, and along lines of constant η at $\eta = 0$, (the centre line), 0.5 and 0.8 by broken lines in Fig.6. We return to these results in section 3.2.

2.5 Calculation of lift, moment and cross loading

The overall lift coefficient C_L, pitching moment C_m and lengthwise distribution of cross loading $\bar{\ell}(x)$ can be obtained by integrating the load over the wing planform.

The lengthwise distribution of cross loading $\bar{\ell}(x)$ is given by

$$\bar{\ell}(x) = \frac{1}{S} \int_{-s(x)}^{s(x)} \ell(x,y)\,dy$$

$$= \frac{2s(x)}{S} \int_0^1 \ell(x,y)\,d\eta \qquad (2)$$

where S is the planform area of the wing.

The lift coefficient C_L and pitching moment coefficient C_m about the apex are given by

$$C_L = \frac{1}{S} \int_0^1 \int_{-s(x)}^{s(x)} \ell(x,y)\,dy\,dx$$

$$C_m = \frac{1}{S} \int_0^1 x \int_{-s(x)}^{s(x)} \ell(x,y)\,dy\,dx \quad ,$$

where the pitching moment has been referred to the centre line chord, which is of unit length. Substituting from equation (2), we have

$$C_L = \int_0^1 \bar{\ell}(x)\,dx \tag{3}$$

$$C_m = \int_0^1 x\bar{\ell}(x)\,dx \quad . \tag{4}$$

The centre of pressure position $x_{c.p.}$ is given by

$$x_{c.p.} = \frac{C_m}{C_L} \quad .$$

For each spanwise section, the integration of the load across the span was done firstly using the trapezoidal rule, assuming the load at the leading edge to be zero. To obtain a more accurate result, integration was performed using Simpson's Rule and assuming that the load near the leading edge tended to zero like $(1 - \eta^2)^{\frac{1}{2}}$. The difference in $\bar{\ell}$ obtained was less than 2%, except near the apex and trailing edge where $\bar{\ell}(x)$ is itself very small, so that the absolute error was everywhere less than 0.0025.

As a check on the accuracy of the method of integration, the loads according to the linear theory were integrated to give values of $\bar{\ell}(x)$ which were compared with the values of $\bar{\ell}(x)$ calculated directly from the analytical expression given in equation (IV.4) of Ref.6. It was found that the error in the integration by Simpson's Rule was less than 2.5% except close to the apex.

Values of $\bar{\ell}(x)$ at the attachment condition were obtained for the load distribution given by the nonlinear theory [5] and the load distribution obtained from the measured pressure distribution. These values and the analytical values of $\bar{\ell}(x)$ for the linear theory are illustrated in Fig.7.

The lift and pitching moment coefficients were obtained from equations (3) and (4) by integrating the values of $\bar{\ell}(x)$ and $x\bar{\ell}(x)$ with respect to x along the length, using the trapezoidal rule and assuming that $\bar{\ell}(x)$ is zero at the apex and trailing edge.

2.6 Calculation of drag

One design requirement for the wing was that it should have low vortex drag at the attachment condition. Accordingly during the design process a spanwise distribution of chord loading was chosen that was fairly close to the elliptic distribution which is the optimum for inviscid attached flow.

We discuss drag in terms of a lift-dependent drag factor K where

$$K = \pi A \frac{\left(C_D - C_{D_O}\right)}{C_L^2} \quad , \tag{5}$$

where C_D is the drag coefficient of the wing at lift coefficient C_L and C_{D_O} the drag coefficient of the unwarped wing of the same planform and thickness distribution at zero incidence. The lift distribution chosen for the design corresponds to a lift-dependent drag factor K of 1.099, which is close to the theoretical minimum of unity for planar wings in attached flow. However, the measured drag factor at the attachment condition, based on the balance measurements of Ref.2, was much higher, being 1.32. The value of K given by the nonlinear theory[5] would therefore be of great interest, and an attempt was made to calculate this from the pressure distribution over the wing.

The drag coefficient C_D is given by

$$C_D = \frac{1}{S} \iint_{S_u - S_\ell} C_p \, dydz \quad , \tag{6}$$

where S_U and S_ℓ denote the upper and lower surfaces of the wing; and for an inviscid flow model, $C_{D_O} = 0$. Therefore

$$\int_{-S} C_p \left.\frac{\partial z}{\partial x}\right|_{y \text{ const.}} dydx \quad . \tag{7}$$

The pressure coefficient is a smoother function of x for fixed η than for fixed y , so it is more accurate to integrate over the surfaces with respect to x and η . Since $y = \eta s(x)$ and

$$\left.\frac{\partial 2}{\partial x}\right|_{y \text{ const.}} = \left.\frac{\partial z}{\partial x}\right|_{\eta \text{ const.}} - \frac{\eta}{s}\frac{ds}{dx}\left.\frac{\partial z}{\partial \eta}\right|_{x \text{ const.}}$$

we have

$$\frac{SC_D}{2} = \int_0^1 \left\{ \int_0^1 s(x) C_p(x,y) \left.\frac{\partial z}{\partial x}\right|_{\eta \text{ const.}} dx \right\} d\eta$$

upper surface-lower surface

$$- \int_0^1 \left\{ \int_0^1 \eta C_p(x,y) \frac{ds}{dx} \left.\frac{\partial z}{\partial \eta}\right|_{x \text{ const.}} d\eta \right\} dx \quad . \qquad (8)$$

upper surface-lower surface

The principle guiding the choice of the order of integration was that the integrand should be integrated first in the direction in which it varies most rapidly. In the first integral above it is the behaviour of the integrand near $x = 1$ for constant η that is critical, so the first integration is with respect to x. In the second integral of (8), the critical variation is near $\eta = 1$ and so the first integration is with respect to η. A computer program was written to evaluate each of the double integrals in (8) over the two surfaces by the trapezoidal rule. Values on Roberts' grid were used, and the substitutions

$$x = \tfrac{1}{2}(1 - \cos\psi) \quad , \quad \eta = \sin\theta$$

were introduced, so that the integration points were concentrated where the integrand varied most rapidly, and the integrand was available at equal intervals of ψ and θ over most of the range. After the substitutions, the integrand was assumed to tend to zero as the edges of the planform were approached, since $dx/d\psi = 0$ for $x = 0$ and 1 and $d\eta/d\theta = 0$ for $\eta = 1$.

Unfortunately the points at which reliable values of the pressure coefficient have been obtained are not close enough to the leading edge to define the behaviour of the integrand accurately. This difficulty is illustrated in Figs.8 and 9. In Fig.8 the integrand from equation (7), i.e.,

$$J(x,\eta) = \left\{ C_p \left.\frac{\partial z}{\partial x}\right|_{y \text{ const.}} \right\}_{\substack{\text{upper} \\ \text{surface}}} - \left\{ C_p \left.\frac{\partial z}{\partial x}\right|_{y \text{ const.}} \right\}_{\substack{\text{lower} \\ \text{surface}}} \tag{9}$$

is plotted against η for three values of x. The behaviour of $J(x,\eta)$ near $\eta = 1$ is not well defined and it will clearly have an appreciable effect on the value of the integral of J, especially since J changes sign in the range of integration. A similar difficulty is encountered near $x = 1$ for the quantity $H(x)$, where

$$H(x) = s(x) \int_0^I J(x,\eta)dy \quad , \tag{10}$$

and is shown in Fig.9. Since

$$C_D = \frac{2}{S} \int_0^{\bar{}} H(x)dx \quad , \tag{11}$$

these uncertainties make accurate evaluation of the drag very difficult.

The value of the lift-dependent drag-factor K at the attachment incidence for the nonlinear theory was obtained as 0.99. However in view of the uncertainties mentioned above this value could be 20% or more in error, and so no meaningful comparison with linear theory or experiment is possible.

3 RESULTS

3.1 Lift coefficient, centre of pressure and cross-loading

The wing was designed by linear theory to have a lift coefficient of 0.1 and a centre of pressure at 0.533 of its length from the apex ($x = 0.533$), at the angle of incidence for which the flow was attached.

Balance measurements[2] in the 4ft x 3ft low-speed wind tunnel showed a lift coefficient at this attachment incidence of 0.101 and a centre of pressure at $x = 0.502$. The Reynolds number of these tests was low and so transition was fixed artificially to avoid the occurrence of flow separation from the rear of the model. A larger model was used in the No.2 11½ft tunnel for pressure

measurements [4]. Integration of the pressures measured at the attachment incidence gives a lift coefficient of 0.103 and a centre of pressure at $x = 0.528$. The agreement in lift coefficient is very satisfactory, but the discrepancy in centre of pressure position is still under investigation. Further details are given in Refs.2 and 4.

The nonlinear theory of Roberts and Rundle could be expected to give more accurate results than the linear theory, especially near the apex, where the cross-sections are thicker. Integration of the pressures due to the nonlinear theory over the wing gives a CL of 0.109 and an $x_{c.p.}$ of 0.556. The results for the lift coefficient and $x_{c.p.}$ can be summarised in a table:

	Linear theory	Roberts' nonlinear theory	Experiment-balance measurement	Experiment, by integration of pressures
C_L	0.1	0.109	0.101	0.103
$x_{c.p.}$	0.533	0.556	0.502	0.528

The differences in the values of C_L and $x_{c.p.}$ obtained from the three sources can be clarified by consideration of the lengthwise distribution of cross-loading illustrated in Fig.7. This shows that the nonlinear theory is in very good agreement with the experimental values from the apex back to $x = 0.75$. However, it predicts much more load near the trailing edge than is present according to the experiment, thus giving larger values for both C_L and $x_{c.p.}$. This effect is presumably largely due to the fact that the calculation is for a potential flow and no account has been taken of viscous effects.

The linear theory values for the cross-loading are in reasonable agreement with the experimental values until $x = 0.7$, although as expected, they underestimate the experimental values near the apex. The linear theory also appears to give reasonable agreement with the experimental values for x greater than 0.85, but examination of the spanwise load distributions (Fig.5b) in this region shows that this agreement is probably fortuitous (see also section 3.2).

Results from slender-body theory and its fully-linearized form, slender thin-wing theory, are presented in Appendix B in order to confirm the source

of the extra lift acting near the wing apex. This is shown to arise, within the slender approximation, from the association of appreciable thickness and appreciable cross-sectional camber.

3.2 The load distribution

A comparison of the loads according to the two theories and the experiment is given in Figs.5 and 6. Figs.5a and b show the spanwise variation of the load for the spanwise sections $x = 0.1$, 0.3, 0.5, 0.7 and 0.9 , and Fig.6 shows the variation of load with x for $\eta = 0$ (i.e. along the root-chord), $\eta = 0.5$ and $\eta = 0.8$.

This comparison shows that the loads predicted by the nonlinear theory [5] agree closely with those measured in the experiment, except at cross-sections behind $x = 0.8$, where the experimental values are likely to be affected by the presence of the boundary layer.

The loads predicted by the linear theory agree less closely with the other two load distributions. The underestimation of the load near the apex by the linear theory is marked, and again the loads do not agree near the trailing edge. At other spanwise sections, the linear theory gives less load at the mid-semi-span than measured by experiment, but predicts the peak load to be further outboard than either the nonlinear theory or the experiment. In the integration of the local load to give the cross load $\bar{\ell}(x)$, these effects tend to cancel, thus producing a somewhat fortuitously good agreement between the values of $\bar{\ell}(x)$ calculated from linear theory and measured in the experiment.

3.3 The pressure distribution

The spanwise pressure distributions on sections $x = 0.2$, 0.5 and 0.8 are shown for both theories and the experiment in Figs.10a and b. Fig.10a confirms the close agreement between the nonlinear theory and the experiment near the apex. Elsewhere (Fig.10b) the detailed agreement between the pressure distributions is poorer than that between the load distributions. On the upper surface of the wing, the pressures given by the nonlinear theory are generally much closer to the experimental values on the outer part cf the wing than the pressures given by the linear theory, which agree better with the experimental values near the root.

On the lower surface of the wing, the variation of the pressures measured experimentaliy across the span is predicted better by the nonlinear theory than

by the linear theory, but towards the rear of the wing the values of the pressure coefficient given by linear theory are in closer agreement with experiment than those given by the nonlinear theory over most of the section, except near the leading edge. This lack of agreement near the leading edge is to be expected since, as the leading edge is approached, the behaviour of the linear theory pressure is dominated by the logarithmic singularity in the pressure due to thickness.

An investigation was carried out to see whether the addition of second-order terms in the pressure coefficient determined by linear theory would produce results in closer agreement with the nonlinear results and the experiment. The pressure coefficient was calculated using Bernoulli's equation for zero Mach number, so that

$$C_P = -2u - (u^2 + v^2 + w^2) \qquad (12)$$

where u, v and w are the disturbance velocities according to linear theory in the x, y and z directions, non-dimensionalised with respect to the free-stream velocity; whereas the usual linear theory expression for the pressure coefficient is

$$C_P = -2u \quad . \qquad (13)$$

The pressure distributions so obtained at two typical cross-sections are shown in Fig.11. These show that the inclusion of the second-order terms in equation (12) does not give any consistent improvement. It is presumably necessary to include also the second-order terms introduced through the boundary conditions, as proposed by Weber[7], to obtain a consistent improvement over the wholly linear theory.

3.4 Effect of incidence

The results of the calculation of Roberts and Rundle are available for an incidence of one degree above the attachment incidence, as well as at the attachment incidence, and so the effects of an increase in incidence according to the nonlinear theory can be examined. No reliable numerical method for solving the integral equation of linear theory for the effect of incidence on a slender wing in subsonic flow exists so far, though one is being developed by

Hewitt and Kellaway[8]. In the real flow, separation from the leading edge was found at a small incidence above the attachment condition, and is not represented in these theoretical models. For the present, attention is confined to the results of Roberts and Rundle.

Fig.4a shows that, near the apex, the increment in pressure coefficient due to an increase in incidence is almost uniform across the lower surface. The increment in suction on the upper surface is on average of the same size, but increases from the centre line to the leading edge. Further aft, Fig.4b, the increment in lower-surface pressure also rises towards the leading edge. Over the rear part of the wing, Fig.4c, the increment in pressure on the lower surface falls close to the leading edge, actually becoming negative at $x = 0.9$, presumably reflecting the existence of flow round the leading edge. At successive rearward sections, the increment in suction on the upper surface is concentrated more and more on the outboard part of the wing. Surprisingly there is even a loss in upper-surface suction near the centre line at $x = 0.9$ due to an increase in incidence.

The increase in the local load due to a one degree increase in incidence, $\Delta\ell$, according to Roberts and Rundle, is given in Fig.12 for several cross-sections. Also shown for comparison is the increase in load according to the slender thin-wing theory of R.T. Jones', which is the same as the load on a plane wing, i.e.

$$\ell(x,\eta) = 4\alpha \frac{ds}{dx} \frac{1}{\sqrt{1-\eta^2}} \quad , \tag{14}$$

where α is the increment in incidence (in radians).

Near the apex, the incremental load according to the nonlinear theory is nearly constant across the span, but further aft it increases markedly outboard from the centre line, finally falling as the leading edge is approached on the more rearward sections. The slender thin-wing theory also predicts the outboard rise in load on the thinner cross-sections, but near the leading edge its predictions are dominated by the singular behaviour of (14). Because the wing has a streamwise tip, with $ds/dx = 0$ at $x = 1$, the predictions of the slender theory do not deteriorate appreciably as the trailing edge is approached.

The lift, moment and cross loading for the theory of Roberts and Rundle at one degree above attachment have been calculated as described in section 2.5, and the lengthwise distribution of cross-loading is shown in Fig.13. The lift coefficient has increased to 0.139 (*cf.* section 3.1) and the position of the centre of pressure has moved only slightly to $x = 0.558$. Thus the lift slope $\partial C_{L_I} / \partial \alpha$ is 1.736 compared with the experimental value[2] of 1.574 and the slender thin-wing theoretical value of $\frac{1}{2}\pi A = 2.175$. The nonlinear theory gives the position of the aerodynamic centre at $x = 0.568$ compared with the experimental value[2] of $x = 0.543$ and the slender thin-wing theory value of 0.563, obtained from (14). Since the slender theory is substantially in error in its prediction of lift-slope, its agreement with the nonlinear theory for aerodynamic centre must be regarded as accidental. As was found for the attached flow condition, section 3.1, the nonlinear inviscid flow calculation predicts rather too much lift, occurring rather too far aft, as would be expected from its neglect of boundary-layer effects.

The real flow separates from the leading edges of the wing at angles of incidence different from the attachment incidence, giving rise to further non-linearities in the aerodynamic loading. This separation is not represented in the theoretical models applied in the present comparisons, which are therefore confined to the immediate neighbourhood of the attachment incidence.

4 CONCLUSIONS

At the design incidence, at which experiment [1,2] confirmed that attached flow was obtained, the linear theory design method [3] gives:

(a) Practically the same value for the lift coefficient as that measured in the experiment[2], but a significantly lower value than that given by the nonlinear inviscid calculation[5]. This is apparently because viscous effects in the real flow reduce the lift below the inviscid value, which is underestimated by the linear theory.

(b) An inadequate estimate of centre of pressure. The linear theory predicts the centre of pressure to lie 2% of the centre-line chord further forward than the nonlinear theory. However, losses of lift at the rear of the wing due to viscous effects cause the experimental position to be ahead of both theoretical predictions.

(c) A fair approximation to the lengthwise distribution of cross-loading. The linear theory underestimates the cross-loading near the apex, where

the sections are thick and cambered. Further aft the situation is less clear, but near the rear the linear theory is predicting much less lift than the nonlinear inviscid theory, which itself substantially over-estimates the measured loading [4].

(d) Local loads and pressures to fair accuracy. Inclusion of second-order terms, calculated by linear theory, in the relation for the pressure coefficient fails to give any consistent improvement.

The nonlinear calculation of Roberts and Rundle[5] predicts the local pressures measured experimentally at the design incidence very closely over most of the wing, except near the trailing edge, where substantial differences are introduced, apparently by viscous effects. Values for the overall characteristics of the wing - lift, centre of pressure, lift-slope and aero-dynamic centre - are therefore not given correctly. The information obtained from the calculation was not sufficient to provide a useful estimate of the lift-dependent drag at the design incidence.

The next step would be to see whether a calculation of the growth of a three-dimensional boundary layer would resolve the differences between the inviscid theory and the experiment.

Appendix A

DETAILS OF ROBERTS' GRID

Roberts' grid consists of 17 lines of constant x and 11 lines of constant η, and is shown on the right-hand side of **Fig.1.** The values of x are 0.00541, 0.01498, 0.03806, 0.08427, 0.14644, 0.22222, 0.30866, 0.40246, 0.5, 0.59754, 0.69134, 0.77778, 0.85356, 0.91574, 0.96194, 0.98502 and 0.99459. The values of x between 0.03806 and 0.96194 are given by the formulae

$$x = \frac{1}{2}\left(1 - \cos\frac{n\pi}{16}\right) \qquad \text{for } n = 2 \text{ to } 15 \ . \tag{15}$$

The values of η are 0.0, 0.1305, 0.2588, 0.3827, 0.5, 0.6088, 0.7071, 0.7933, 0.8660, 0.9239 and 0.9659. These values of η are given by

$$\eta = \sin\left(\frac{m\pi}{24}\right) \qquad \text{for } m = 0 \text{ to } 10 \ . \tag{16}$$

Appendix B

LIFTING EFFICIENCY OF THICK, CAMBERED SLENDER WINGS

A feature of the results reported here is that the apex region of the wing produces more lift, both in the wind tunnel and in the nonlinear inviscid calculation, than was expected on the basis of the fully linearized design method. This Appendix shows that this result is consistent with the available analytical solutions based on the slender body approximation. The relation between the various theoretical models involved, all of which treat an inviscid, attached flow, is conveniently represented in a table:

Differential equation:	$\phi_{YY} + \phi_{zz} = 0$	$(1 - M^2)\phi_{xx} + \phi_{yy} + \phi_{zz} = 0$
Boundary condition:		
in a mean plane	slender thin-wing theory	subsonic linear theory (e.g. Ref.3)
on the body surface	slender body theory (e.g. Ref.10)	surface singularity methods (e.g. Ref.5)

The design process used[3] for the wing tested proceeded from a warp surface designed by subsonic linear theory to have a certain lift coefficient with attached flow at the leading edges and added a volume distribution in a direction normal to the local cross-section of the warp surface. To use the analytic results of Portnoy [10] for a slender half-cone, we have to invert the process, obtaining a warp surface by proceeding equal distances along inward normals from the upper and lower surfaces of the half-cone. By a familiar result in the theory of conic sections, the cross-sections of the warp surface obtained in this way are parabolic arcs. The forward and inverse processes are not exactly equivalent, in the sense that applying them successively does not regenerate the original surface, but it is proved in Appendix B of Ref.3 that they are equivalent to second order in the wing thickness. In this Appendix it is shown that the use of slender-body theory for the half-cone [10] predicts more lift than the use of slender thin-wing theory for the parabolic-arc warp surface, just as the surface-singularity method of Roberts and Rundle[5] predicts more lift on the thick cambered apex of the wing than the subsonic linear theory design method[3].

The results for the half-cone are obtained by taking the limit of Portnoy's equation (28) as the thin wing of his configuration disappears into the body. Then

$$C_L = K^2 M_1 + \alpha K M_2 \quad ,$$

where K is the tangent of half the apex angle of the cone and a is the angle of incidence of the upper, plane, surface. M_1 and M_2 are given by the appropriate limit (Portnoy's parameter $\varepsilon \to 1$) of equation (22) of Ref.10 as

$$M_1 = 4(\pi/\sqrt{3} - 1) \quad , \qquad M_2 = 19\pi/9 \quad .$$

To convert to a half-cone with its lower surface plane and at incidence a , we need to change the signs of C_L and a , giving

$$C_L = \frac{19\pi}{9} K\alpha - 4K^2 \left(\frac{\pi}{\sqrt{3}} - 1 \right) \quad . \tag{17}$$

We can see at once that the lift-curve slope, $\partial C_L / \partial \alpha$, is slightly greater according to slender-body theory, since in the slender thin-wing theory it depends only on the planform and CL = $2\pi K\alpha$ for a plane delta wing. However, we are more concerned with what happens at the incidence for which the flow at the leading edge of the warp surface is predicted to be attached, according to the slender thin-wing theory.

The warp surface with parabolic-arc cross-sections is equivalent to the simplest of the wings for which solutions by slender -thin-wing theory are quoted in Appendix III of Ref.11. The first solution, with suffix 2, refers to a wing whose surface ordinate is given by z_2 , where

$$\frac{z_2}{c_1 s} = -4\eta^2 + 5|\eta| - 2$$

where c_1 is a constant of proportionality. The same solution applies for a wing whose ordinates differ from z_2 by a function of y only, since such a term cannot affect $\partial z/\partial x$. Hence the term in Id in this equation can be omitted to give a wing with parabolic cross-sections:

$$z_2 = -2c_1 s(1 + 2\eta^2) \quad .$$

For the warp surface derived from the half-cone, it is clear that

$$z_2(0) - z_2(1) = s/2 \quad ,$$

so that this particular surface is given by

$$c_1 = \frac{1}{8} \quad . \tag{18}$$

The incidence of the plane containing the leading edge is $-z_2(1)/x$ and so

$$\alpha = 6c_1 s/x = 6Kc_1 = 3K/4 \quad . \tag{19}$$

The lift at this attached flow condition is given by (19) of Ref.11 as

$$C_L = 2\pi c_1 K^2 \quad . \tag{20}$$

The relevant comparison is between the lift coefficient of the warp surface according to slender thin-wing theory, at the incidence for which the flow is attached, given by introducing (18) into (20) as

$$C_L = 0.25\pi K^2 \quad ; \tag{21}$$

and the lift coefficient of the half-cone at the same incidence, according to slender-body theory, given by introducing (19) into (17) as

$$C_L = \pi K^2 \left(\frac{19}{12} - \frac{4}{\sqrt{3}} + \frac{4}{\pi}\right) = 0.547\pi K^2 \quad . \tag{22}$$

The slender-body estimate (22) is over twice the slender thin-wing estimate (21), which is a larger difference than that found between the two estimates in Fig.7 near the wing apex. This is partly because the forward part of the wing is not as extreme in shape as the half-cone. It is also likely that the slenderness assumption over-emphasises the difference.

It should be pointed out that slender-body theory and slender thin-wing theory give the same value for the overall lift of the wing, since, according to both, this only depends on conditions in the plane of the trailing edge, where the cross-section of the wing is just the straight segment assumed in the thin-wing theory.

The increase in lift near the apex depends on a combination of thickness and camber. In general, thick uncambered cross-sections do not produce more lift than thin ones (see e.g. Ref.12 for rhombic sections, unpublished work by E.C. Maskell for biconvex sections and the well-known results for elliptic sections). Highly cambered, thin cross-sections do produce more lift [13] at the attachment condition than the thin-wing approximation would suggest, but this does not account for the present result. Taking a conically cambered wing with a cross-section in the form of a thin circular arc of height equal to a half of its semispan, to compare with the parabolic arc described above, we find the lift according to slender-body theory is given by equation (22) of Ref.13, with $\beta = \frac{1}{2}$, i.e.

$$C_L = \pi(9\alpha K/4 - 23K^2/16) \quad , \qquad (23)$$

where α is the incidence of the plane containing the leading edges. Since the difference between circular-arc and parabolic-arc camber does not affect the theory to the first order in the camber parameter, β, this wing has attached flow according to slender thin-wing theory at the incidence given by (19), and the lift is then given by (23) as

$$C_L = 0.25\pi K^2 \quad ,$$

which is actually identical with the slender thin-wing value (21).

SYMBOLS

A	aspect ratio
C_D	drag coefficient
C_{D_O}	drag coefficient of symmetrical wing at zero lift
C_L	lift coefficient
C_m	pitching moment coefficient, based on centre line chord
C_P	pressure coefficient
c	centre line chord, taken as unit of length
$H(x)$	see equations (IO) and (11)
$J(x,\eta)$	see equation (9)
K	lift-dependent drag factor
L	overall lift
$\ell(x,y)$	local load
$\bar{\ell}(x)$	lengthwise distribution of cross-loading (equation (2))
$\Delta\ell(x,y)$	increase in local load due to 1^o increase in incidence
P	planform parameter: (wing area)/(span × length)
S	planform area
S_u, S_ℓ	upper and lower surfaces of wing
$s(x)$	non-dimensional local semi-span
s_T	non-dimensional semi-span at trailing edge
u,v,w	components of disturbance velocity in x,y,z directions, referred to free stream velocity
x,y,z	non-dimensional Cartesian coordinates, Ox parallel to free stream, Oy to starboard, Oz upwards
$x_{c.p.}$	x coordinate of centre of pressure
α	angle of incidence
η	$y/s(x)$
θ	$\sin^{-1}\eta$
ψ	$\cos^{-1}(1 - 2x)$

REFERENCES

No.	Author	Title, etc.
1	P.J. Butterworth	Low-speed wind-tunnel tests on a family of cambered wings of mild gothic planform of aspect ratio 1.4. ARC CP 1163 (1970)
2	P.J. Butterworth	Further low-speed wind-tunnel tests on cambered mild gothic wings of aspect ratio 1.4. RAE Technical Report to be issued
3	Patricia J. Davies	The design of a series of warped slender wings for subsonic speeds. ARC CP 1263 (1971)
4	P.J. Butter-worth	RAE Technical Report to be issued
5	A. Roberts K. Rundle	Computation of incompressible flow about bodies and thick wings using the spline mode system. ARC 33775 BAC Report Aero MA 19 (1972)
6	M.P. Carr	The calculation of warp to produce a given load and pressures due to a given thickness on thin slender wings in subsonic flow. Handley Page APRO Report 99 (1968)
7	J. Weber	Second-order small perturbation theory for finite wings in incompressible flow. ARC R & M 3759 (1972)
8	B.L. Hewitt W. Kellaway	Developments in the lifting surface theory treatment of symmetric planforms with a leading edge crank in subsonic flow. BAC (MAD) Report AR 313 (1971) DRIC S & T Memo-4-71
9	R.T. Jones	Properties of low-aspect-ratio pointed wings at speeds below and above the speed of sound. NACA Rep. 835 (1946)
10	H. Portnoy	The slender wing with a half-body of revolution mounted underneath. Aeronautical Jour. 72, 803-807 (1968)

REFERENCES (concluded)

No.	Author	Title, etc.
11	J.H.E. Smith K.W. Mangler	The use of conical camber to produce flow attachment at the leading edge of'a delta wing and to minimize lift-dependent drag at sonic and supersonic speeds. ARC R & M 3289 (1957)
12	J.H.B. Smith	Calculations of the flow over thick, conical slender wings with leading-edge separation. ARC R & M 3694 (1971)
13	J.H.B. Smith	The properties of a thin conically cambered wing according to slender-body theory. ARC R & M 3135 (1958)

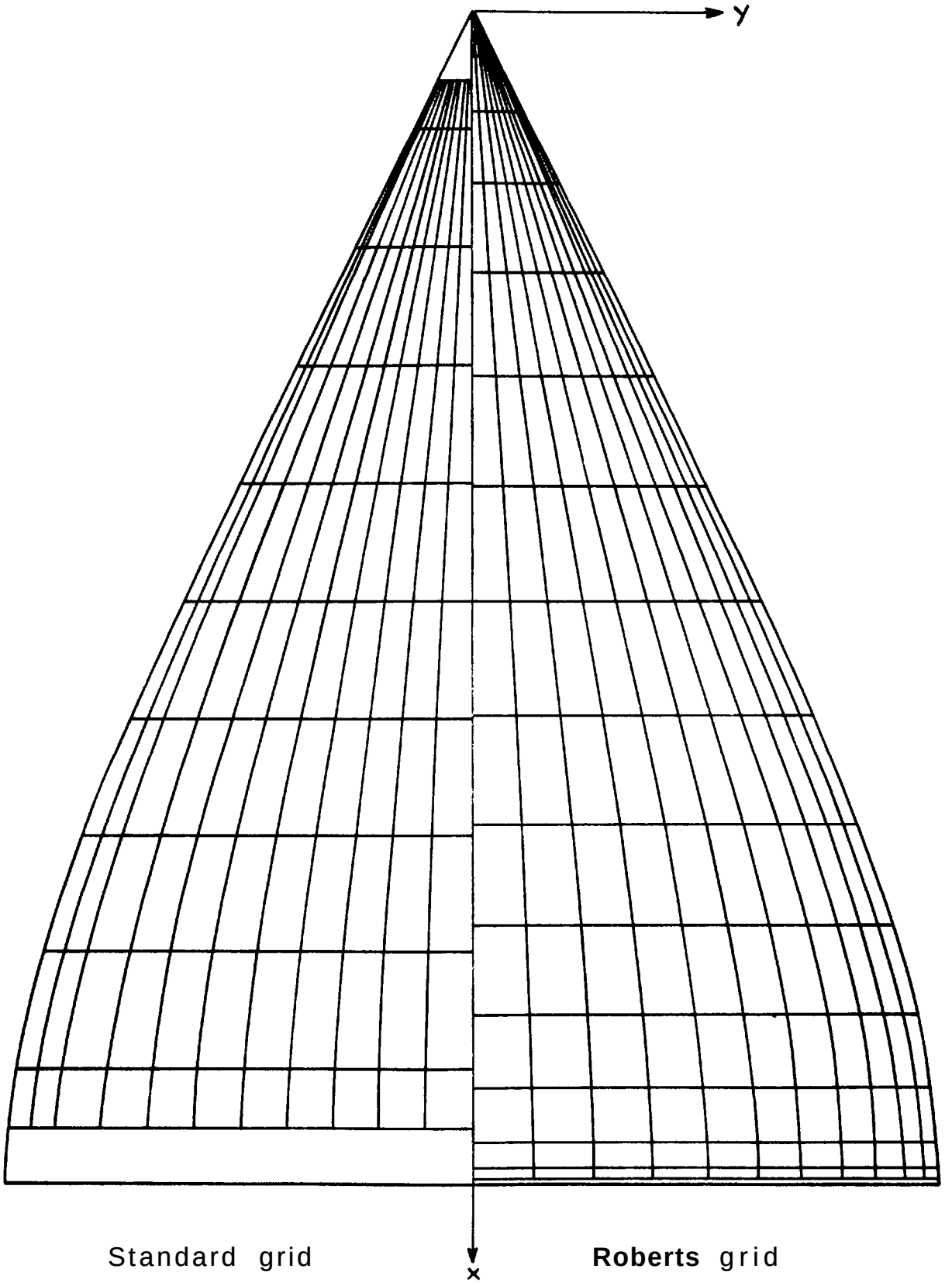

Fig.1 The wing planform, showing the calculation grids

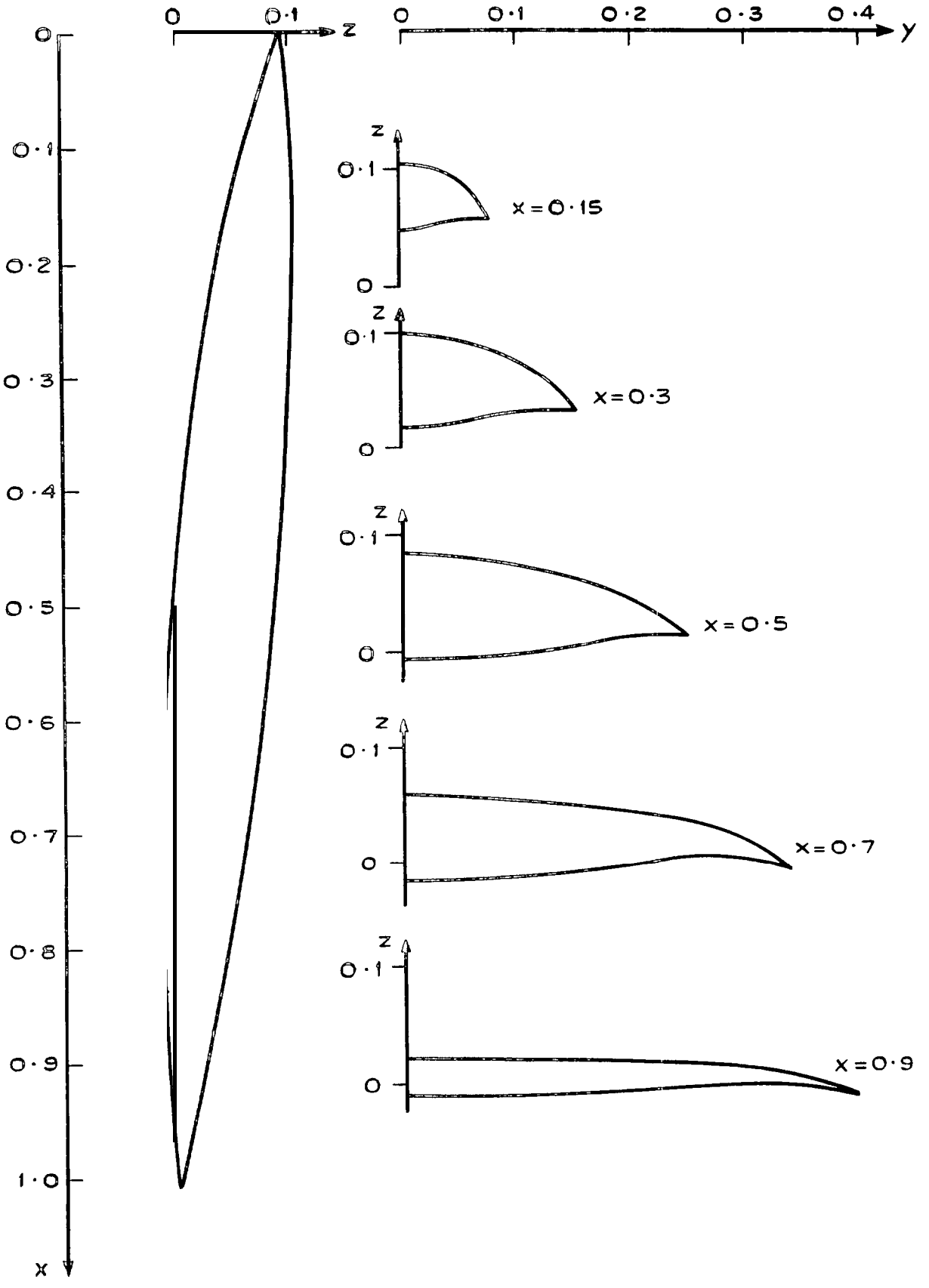

Fig.2 Root chord section, and cross-sections of the wing

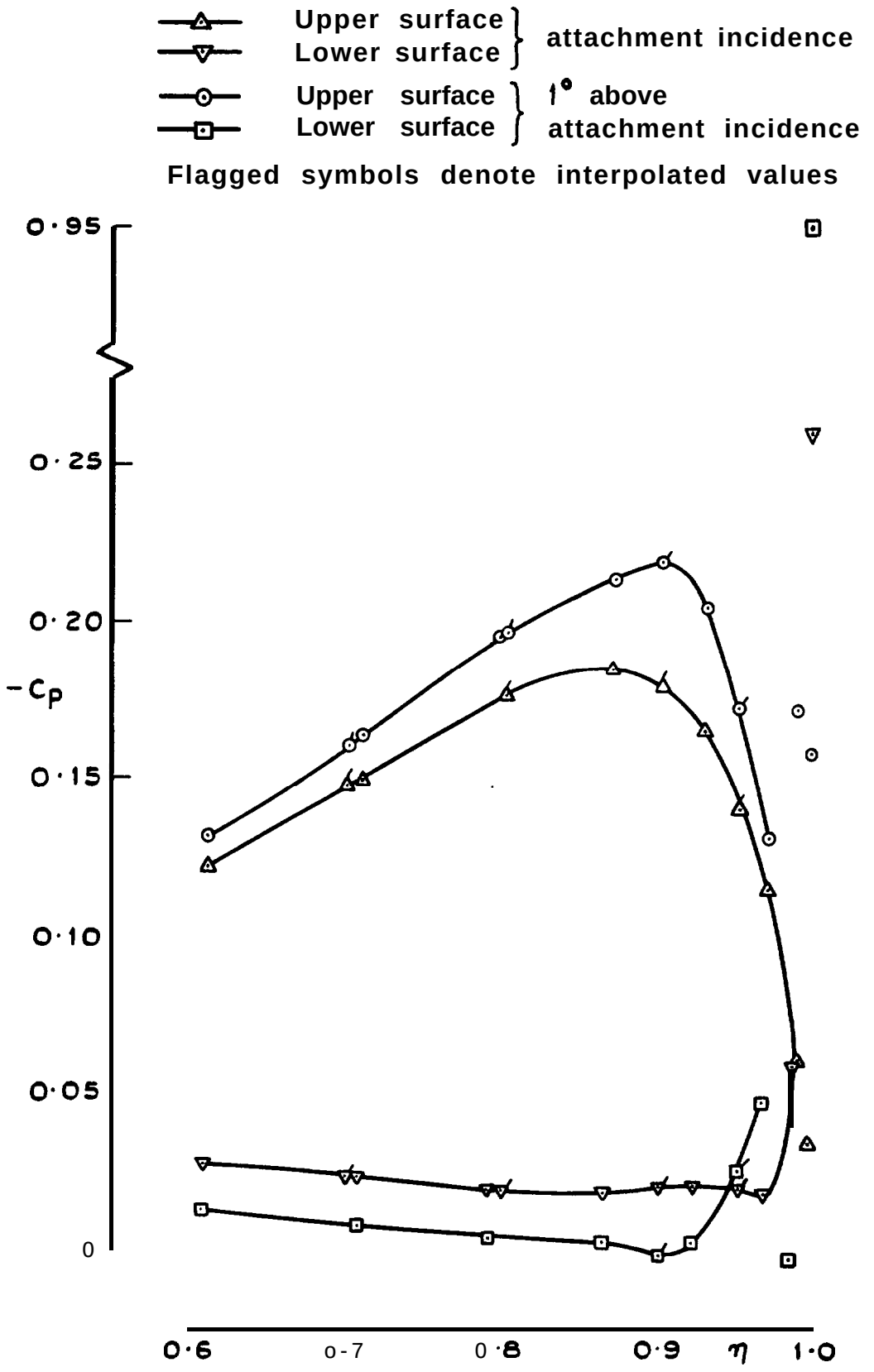

Fig.3 Pressure distributions by the nonlinear theory [5] for the cross-section x=0·8536

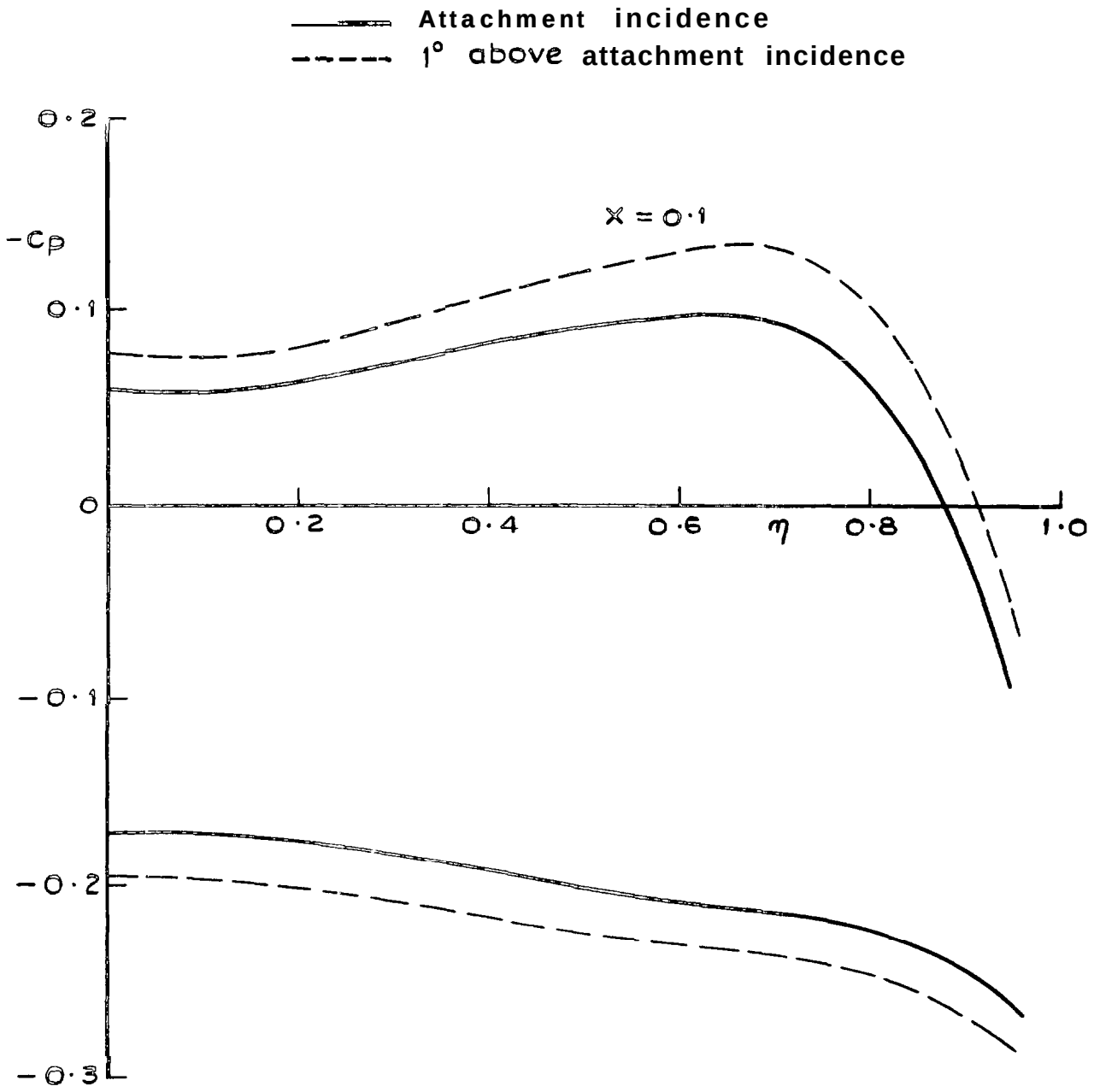

Fig.4a Pressure distribution given by the nonlinear theory [5]

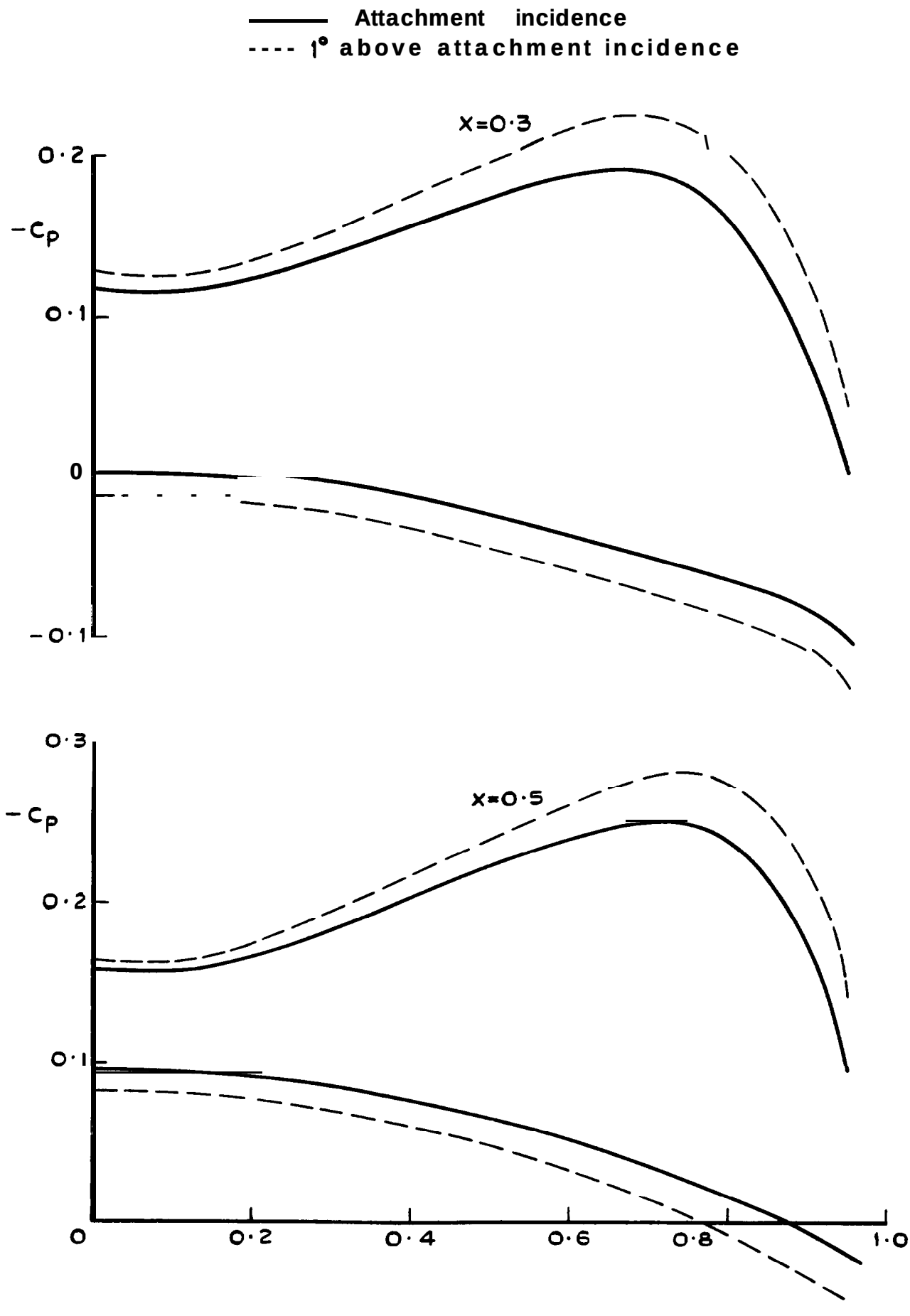

Fig.4b Pressure distribution given by the nonlinear theory5 (ctd)

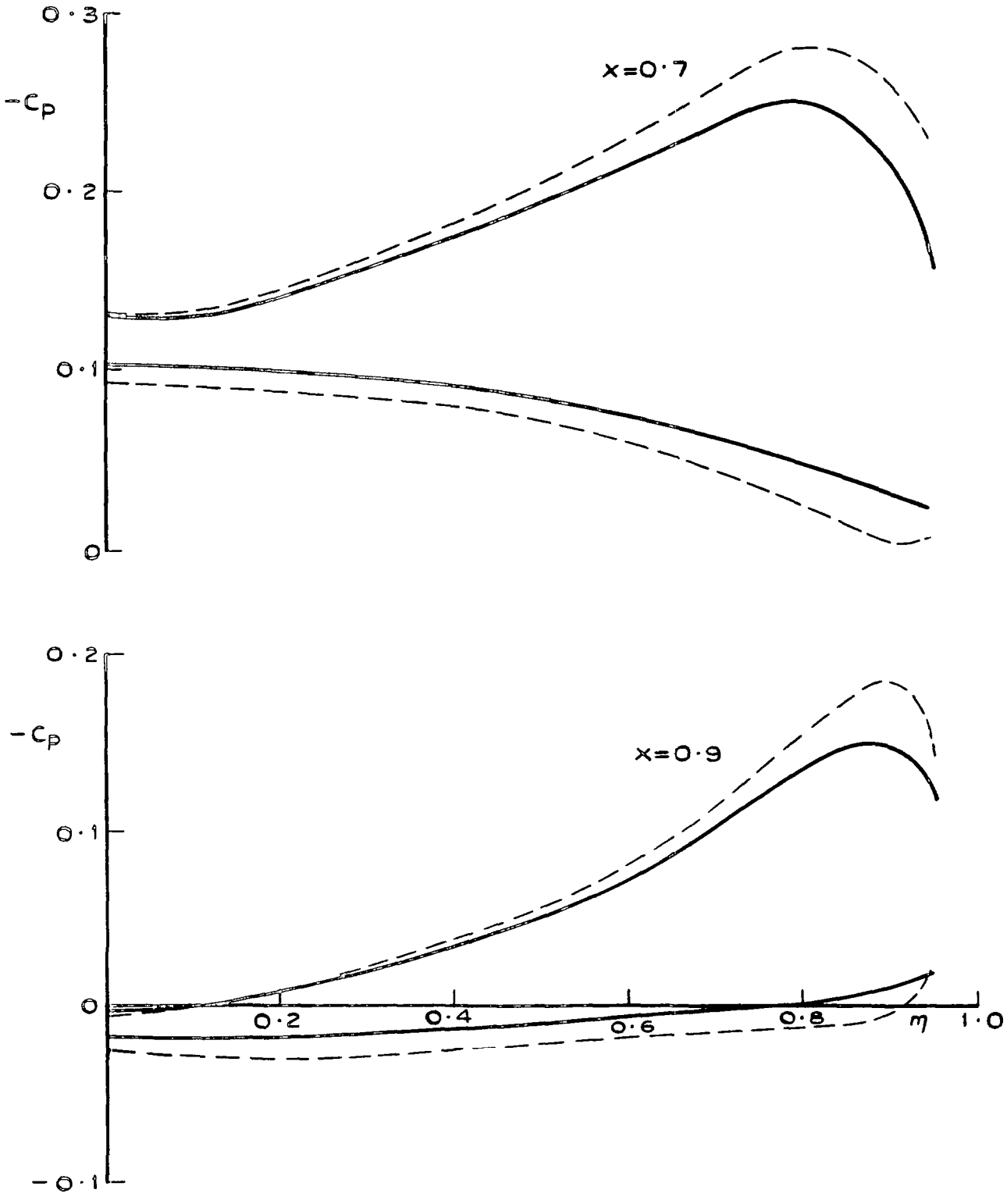

Fig. 4c Pressure distribution given by the nonlinear theory[5] (ctd)

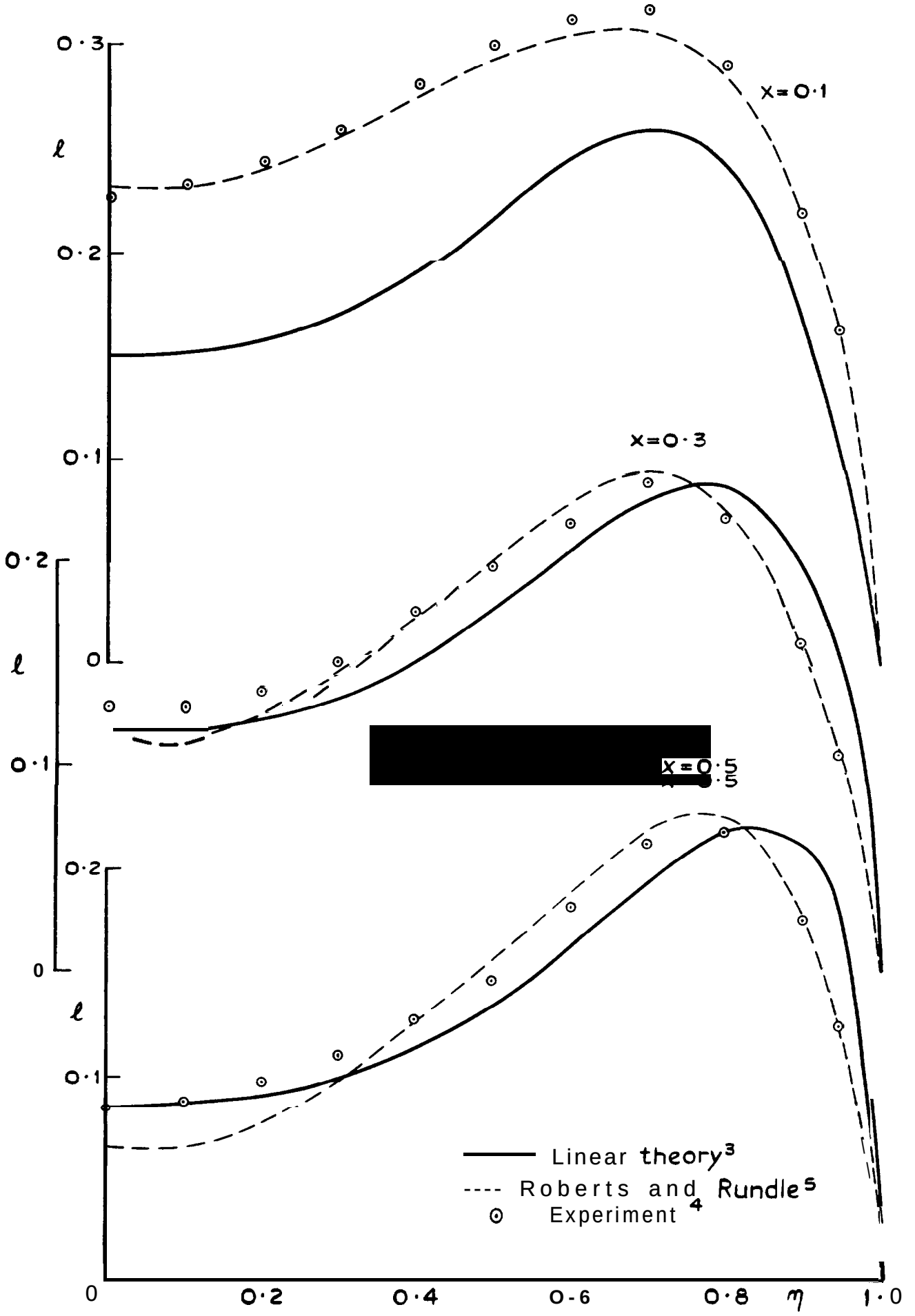

Fig. 5a Load distributions at various cross-sections

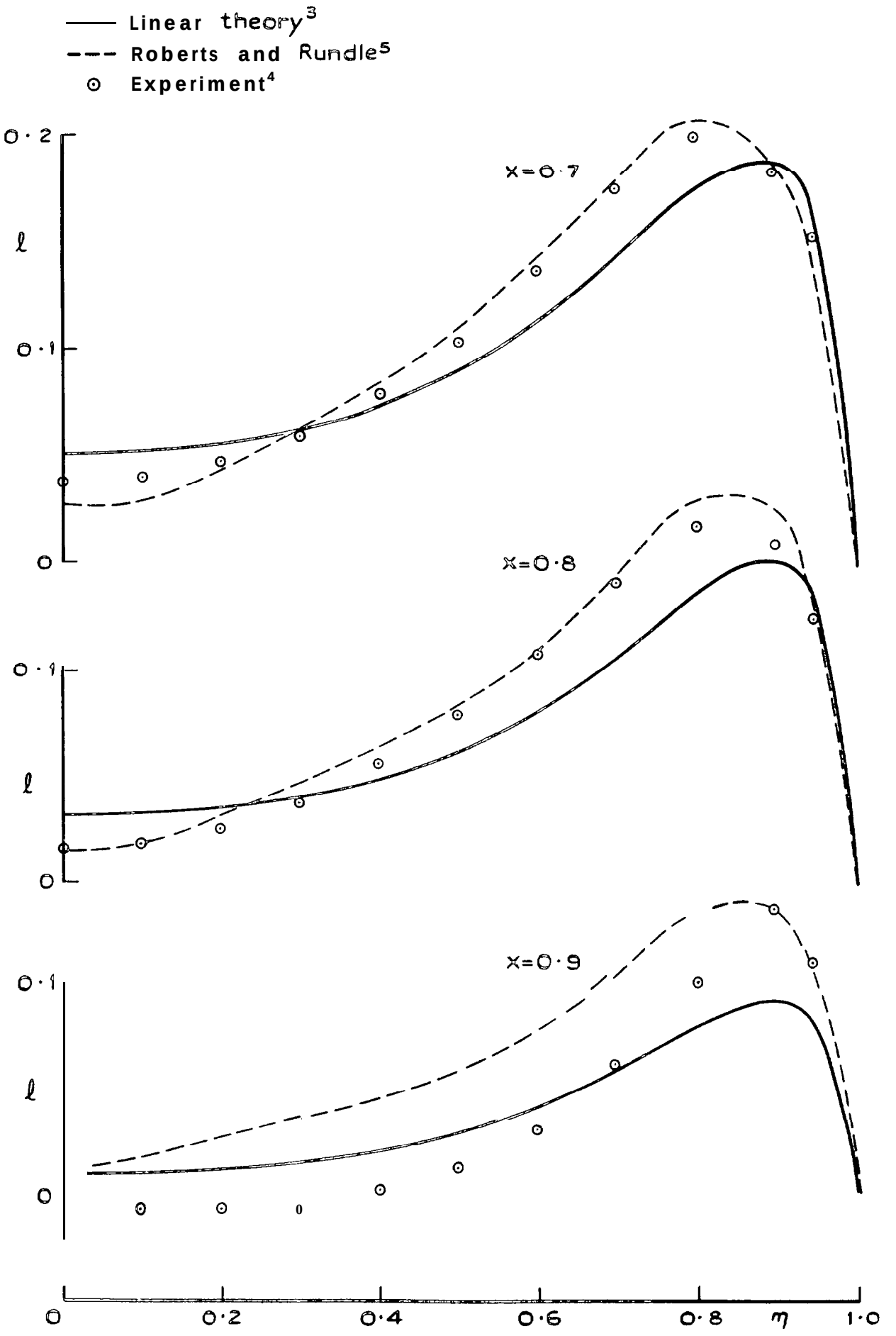

Fig. 5b Load distributions at various cross-sections (ctd)

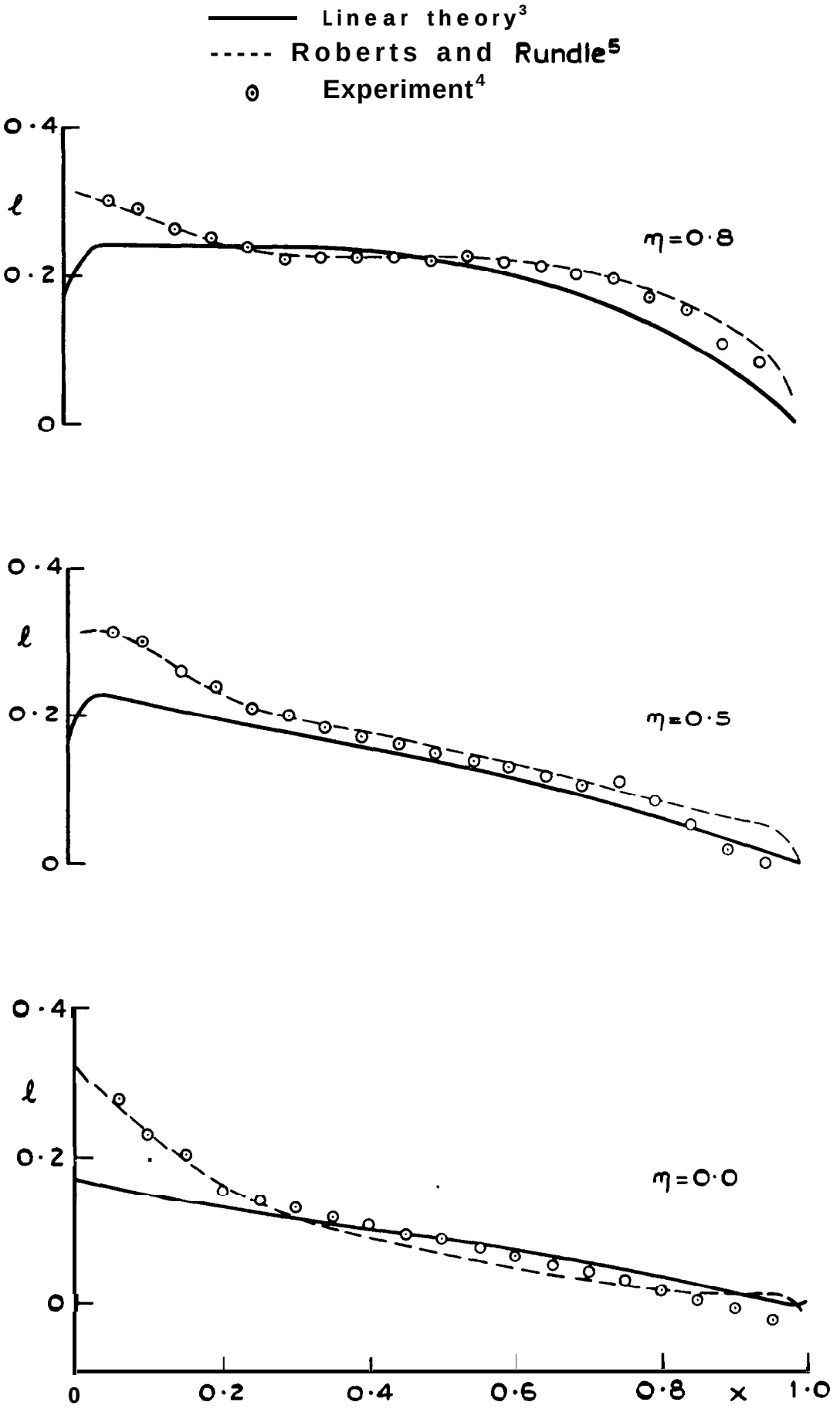

Fig.6 Load distributions on various lengthwise sections

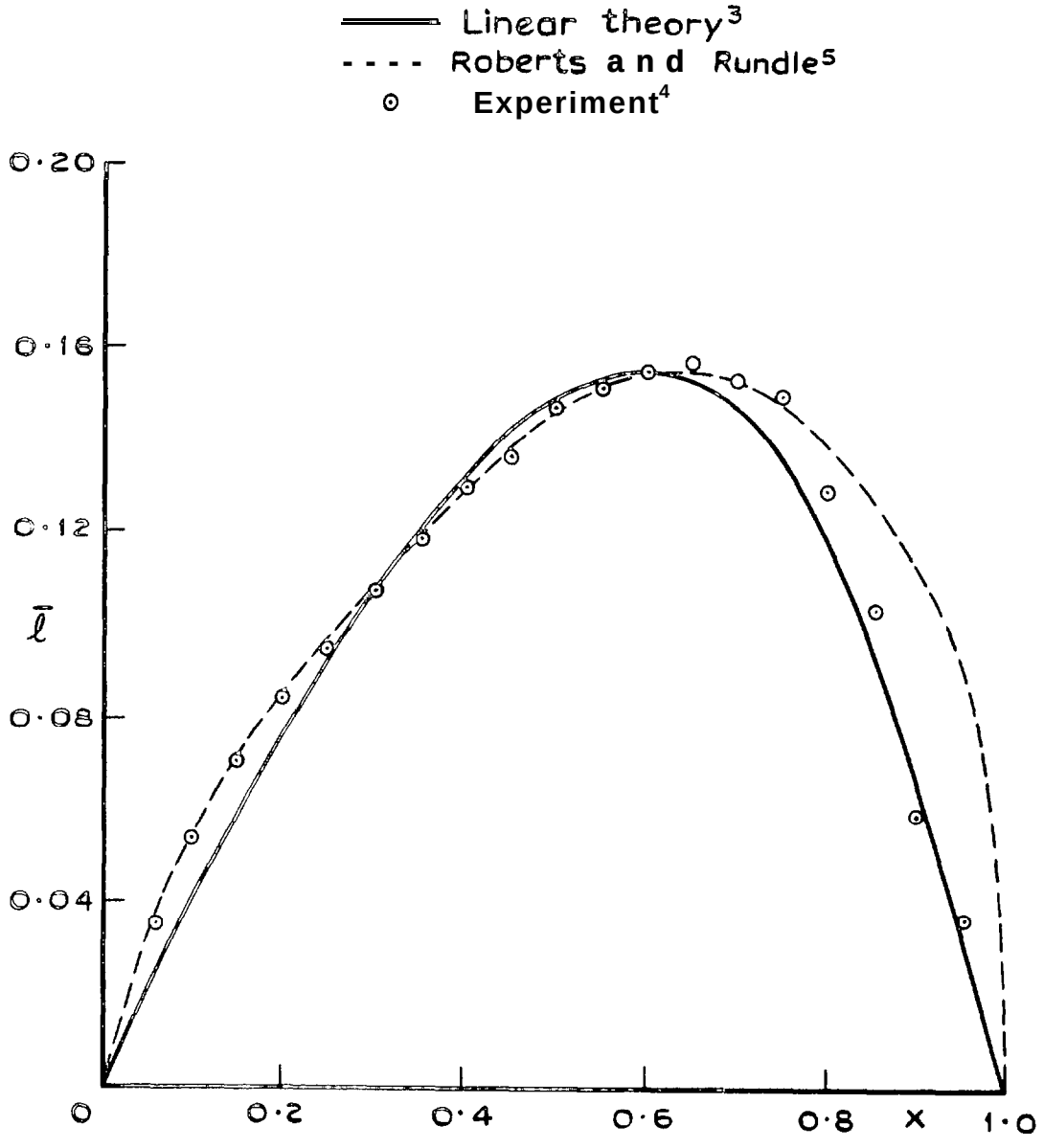

Fig.7 Lengthwise distribution of cross loading

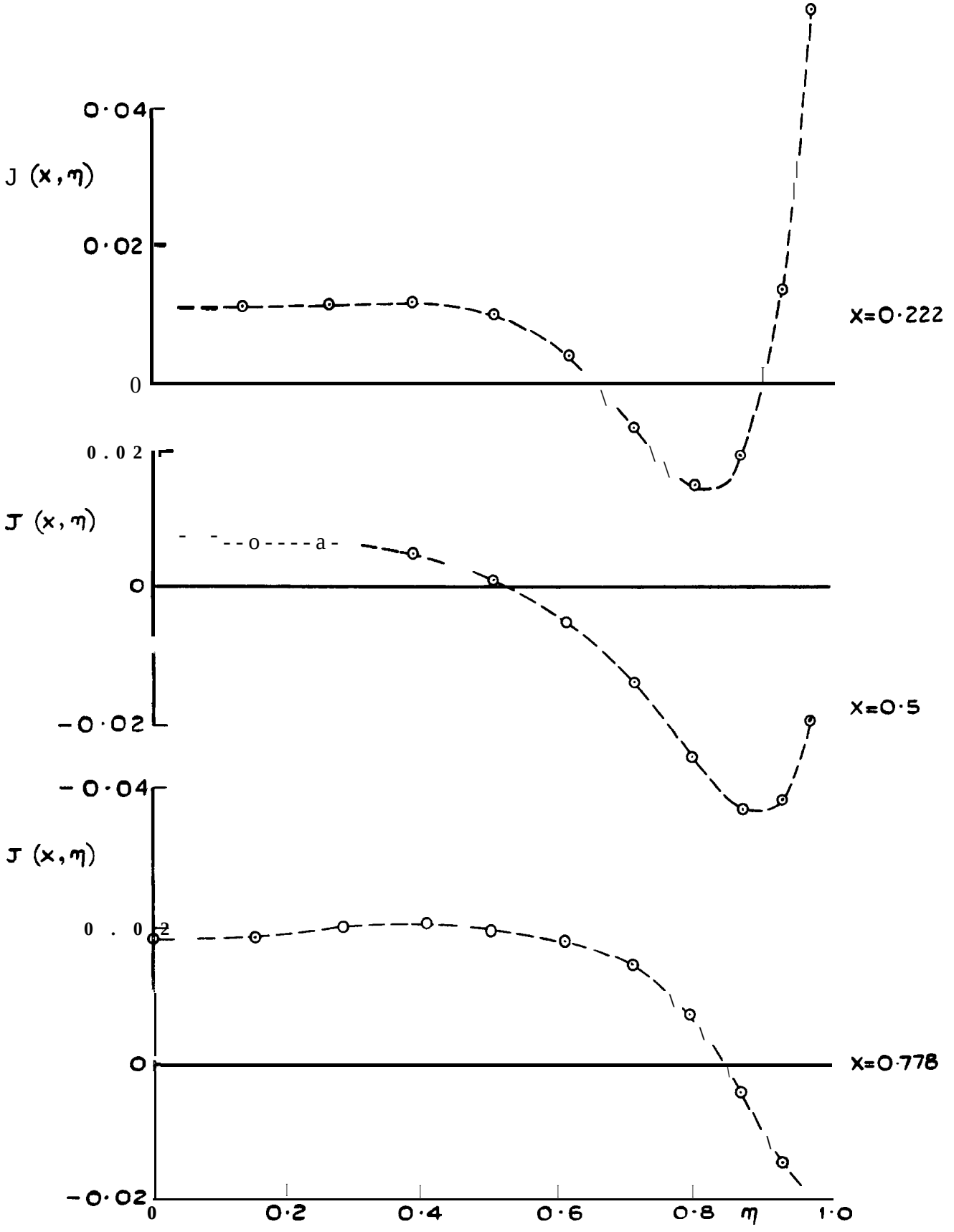

Fig-8 Variation of integrand for drag across span

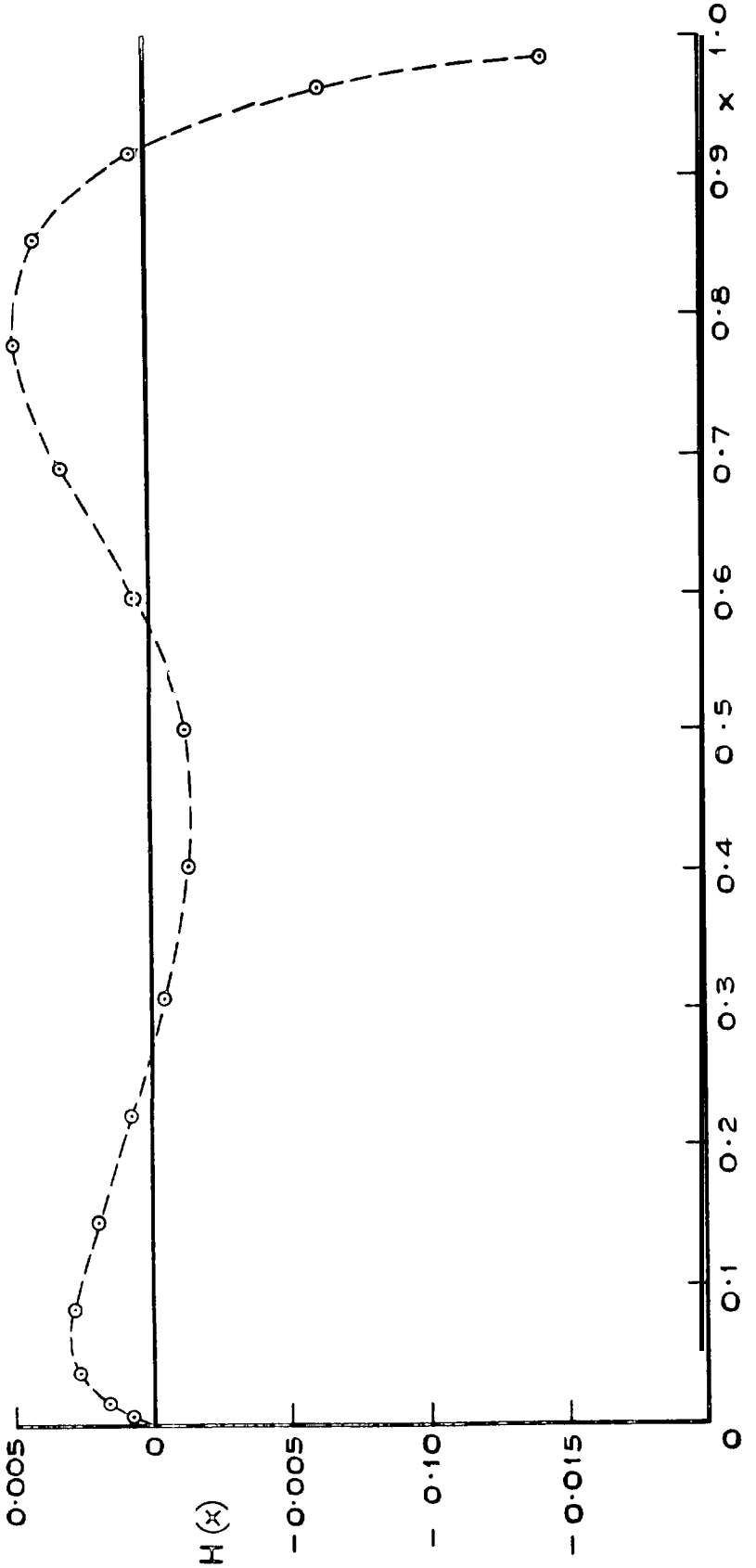

Fig.9 Lengthwise variation of integrand for drag

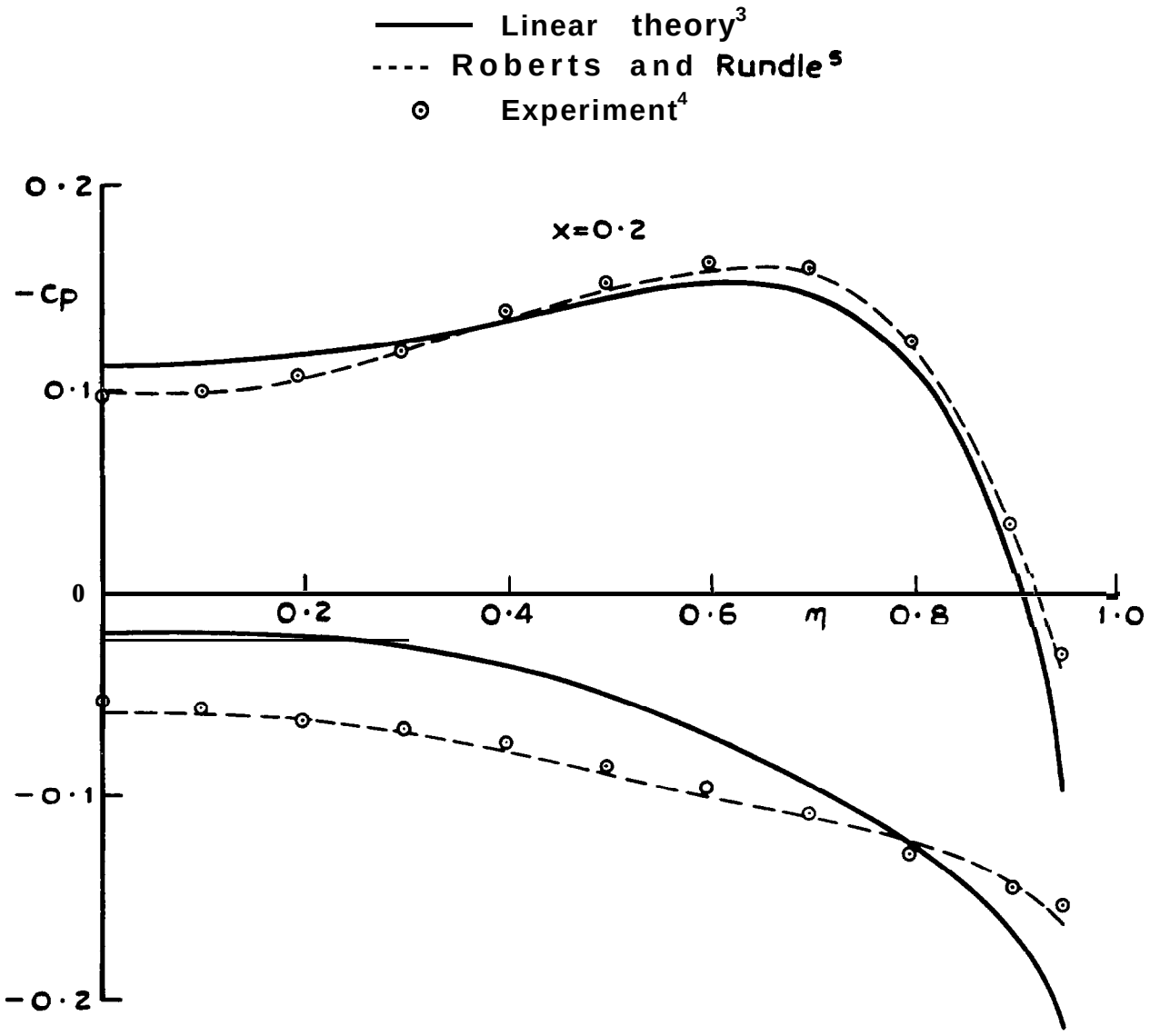

Fig.10 a The pressure distribution on various cross-sections

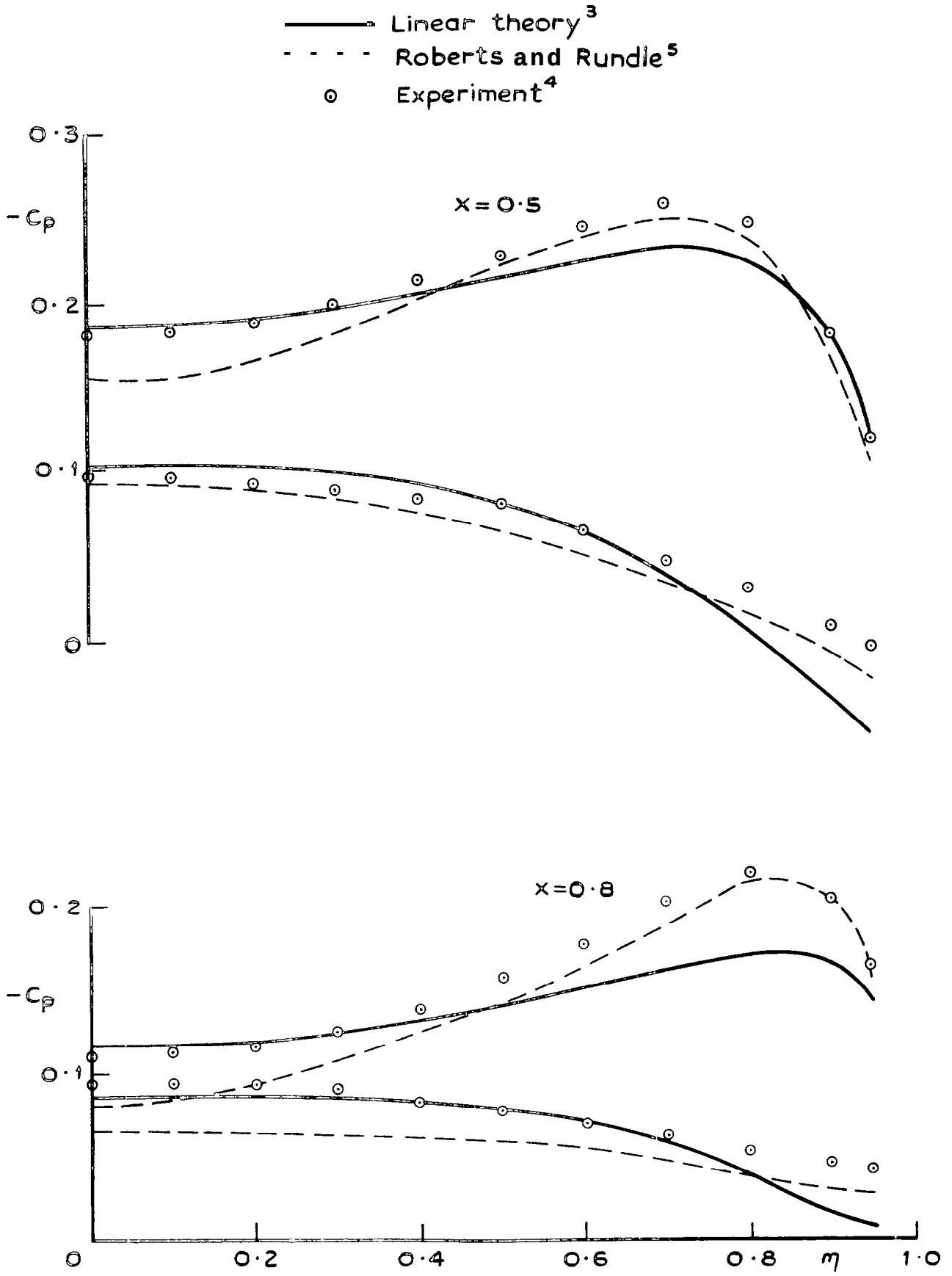

Fig. 10b The pressure distribution on various cross-sections (c td)

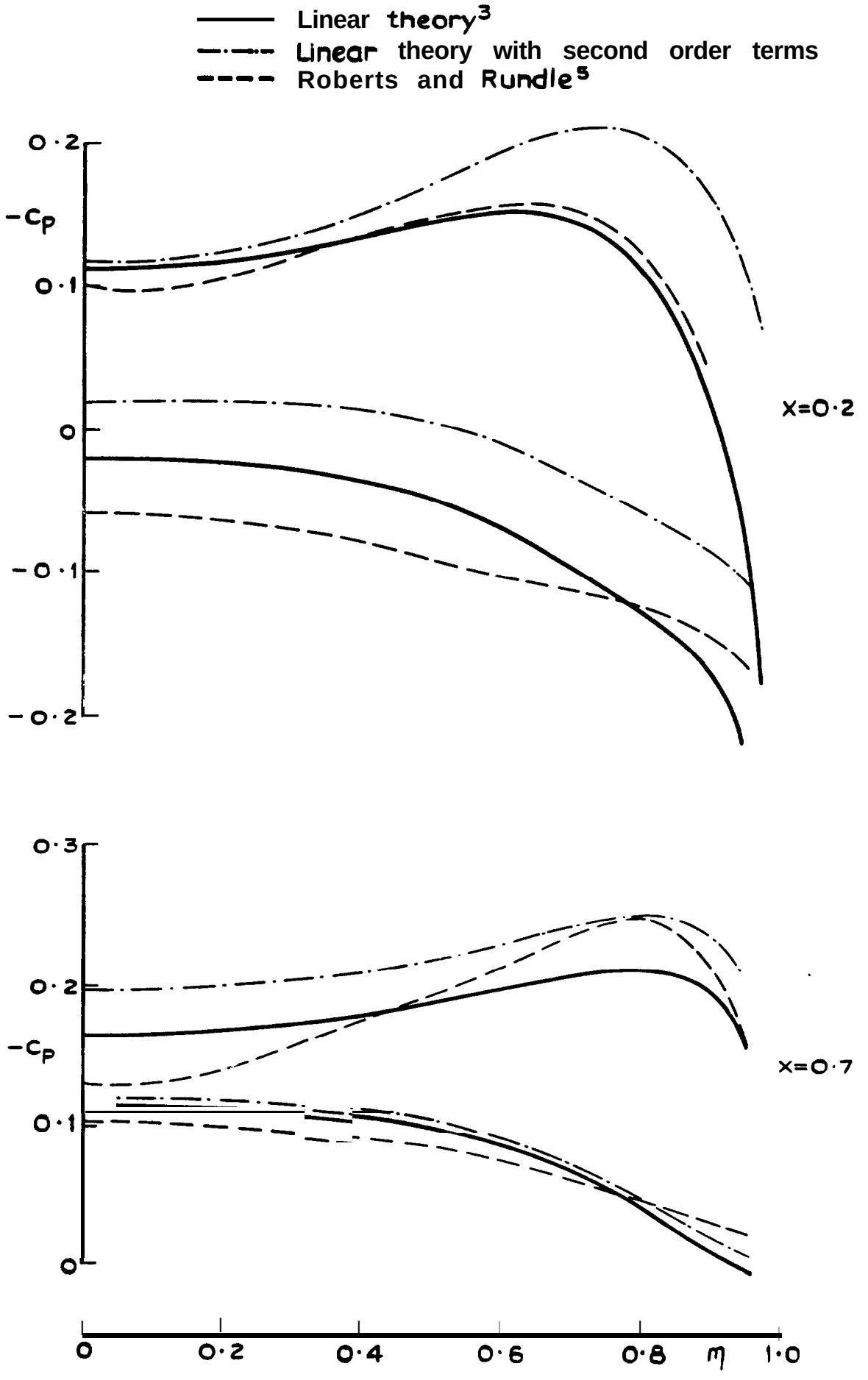

Fig.11 Theoretical pressure distributions at two cross-sections

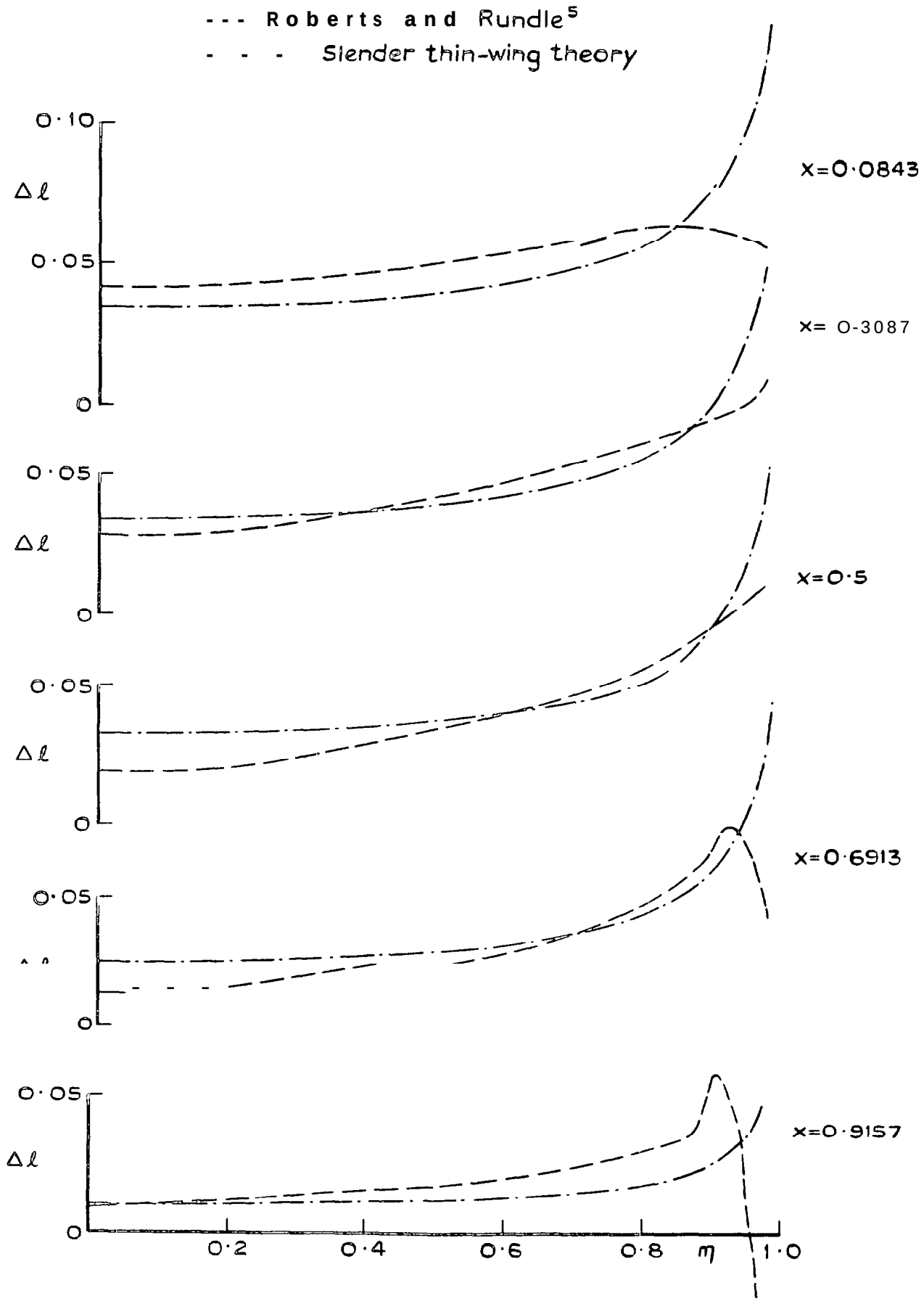

Fig. 12 The increase in load due Po an increase of one degree in the angle of incidence

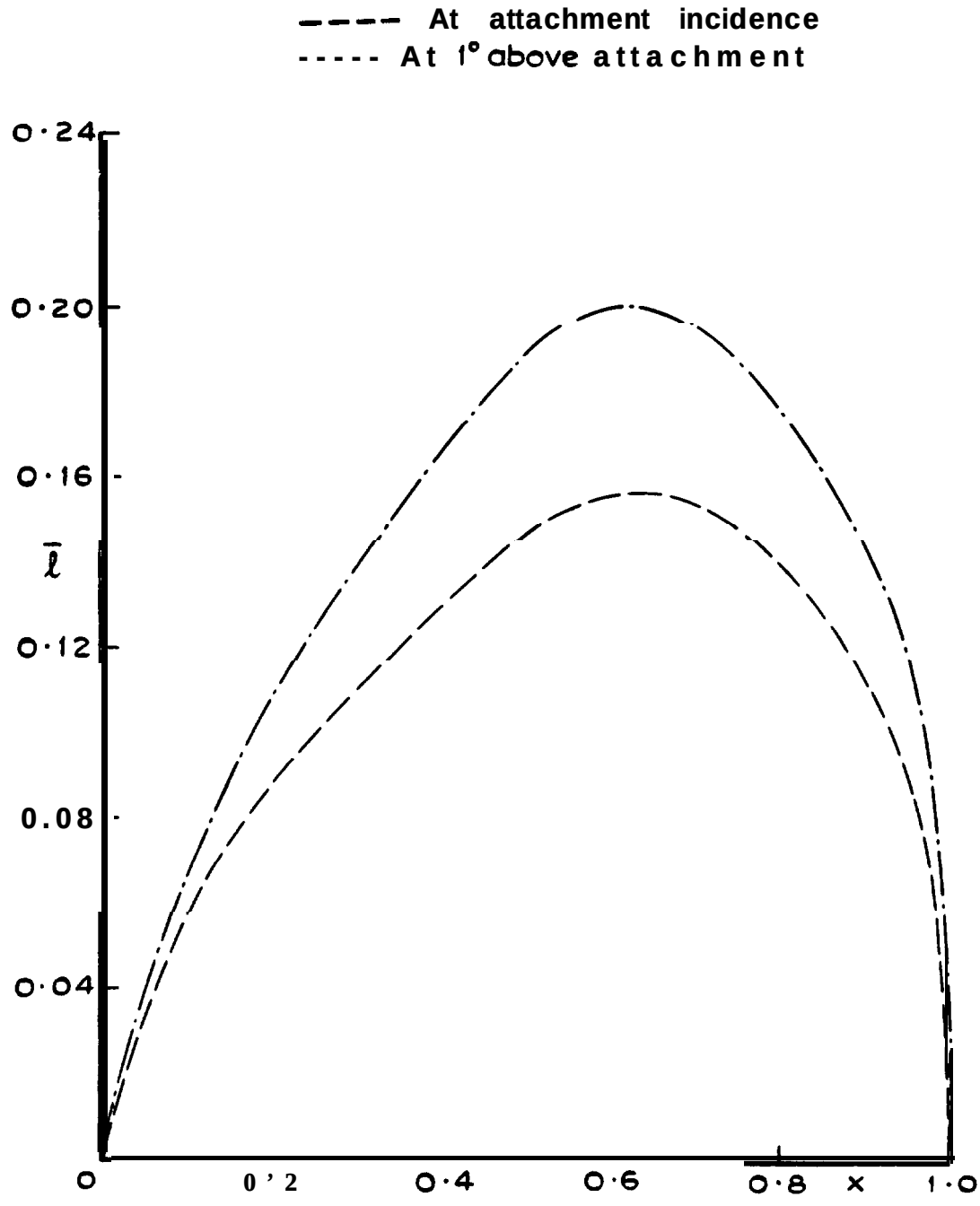

Fig.13 The lengthwise distribution of cross loading given by the nonlinear theory[5]

Produced in England for Her Majesty's Stationery Office by the Royal Aircraft Establishment, Farnborough. Dd. 289030 K4 7/ 75.

ARC CP No.1324
October 1973

Davies, Patricia J.

533.693.3 :
533.6.043.2 :
533.6.013.13 :
533.6.013.12 :
533.6.011.32

AN ASSESSMENT OF THE ACCURACY OF SUBSONIC LINEARIZED THEORY FOR THE DESIGN OF WARPED SLENDER WINGS

A series of warped slender wings has previously been designed using the linearized theory of subsonic flow, as a basis for a systematic experimental investigation of the drag reduction obtainable by warp at low speeds. The force measurements on these wings have now been supplemented by measurements of the pressure distribution over one of them; and the pressure distribution on it has also been calculated for inviscid incompressible flow by a surface-singularity method. This Report compares the distribution of pressure used in the design with those measured and calculated for the design incidence, at which the flow was attached; and assesses the validity of the linear theory. The chief weaknesses are found to be on the thicker cross-sections near the apex, and towards the trailing edge where boundary-layer effects become significant.

Cut here

ARC CP No.1324
October 1973

Davies, Patricia J.

533.693.3 :
533.6.043.2 :
533.6.013.13 :
533.6.013.12 :
533.6.011.32

AN ASSESSMENT OF THE ACCURACY OF SUBSONIC LINEARIZED THEORY FOR THE DESIGN OF WARPED SLENDER WINGS

A series of warped slender wings has previously been designed using the linearized theory of subsonic flow, as a basis for a systematic experimental investigation of the drag reduction obtainable by warp at low speeds. The force measurements on these wings have now been supplemented by measurements of the pressure distribution over one of them; and the pressure distribution on it has also been calculated for inviscid incompressible flow by a surface-singularity method. This Report compares the distribution of pressure used in the design with those measured and calculated for the design incidence, at which the flow was attached; and assesses the validity of the linear theory. The chief weaknesses are found to be on the thicker cross-sections near the apex, and towards the trailing edge where boundary-layer effects become significant.

Cut here

DETACHABLE ABSTRACT CARDS

DETACHABLE ABSTRACT CARDS

Printed and published by
HER MAJESTY'S STATIONERY OFFICE

To be purchased from
York House, Kingsway, London W C 2
423 Oxford Street, London W 1
P O Box 569, London S E 1
13A Castle Street, Edinburgh 2
109 St Mary Street, Cardiff
39 King Street, Manchester 2
Tower Lane, Bristol 1
2 Edmund Street, Birmingham 3
80 Chichester Street, Belfast
or through any bookseller

Printed in Great Britain

P. No. 1324